Orientation of slowly sedimenting fibers in a flowing suspension near a plane wall

By Allan Carlsson[†], Fredrik Lundell[†] & L. Daniel Söderberg[†,‡]

[†]Linné Flow Centre, KTH Mechanics, SE - 100 44 Stockholm, Sweden
[‡]STFI-Packforsk AB, SE - 114 86 Stockholm, Sweden

The effect of a wall on the orientation of slowly sedimenting fibers suspended in a shear flow has been studied experimentally. Experiments were performed at two concentrations with two aspect ratios, $r_p \approx 7$ and $r_p \approx 30$, where r_p is defined as the fiber length divided by the diameter. For all cases the majority of the fibers were oriented close to parallel to the flow direction for distances farther away from the wall than half a fiber length. As the distance from the wall decreased a change in orientation was observed. At distances from the wall closer than about an eighth of a fiber length a significant amount of the fibers were oriented close to perpendicular to the flow. This was particularly clear for the shorter fibers. Due to the density difference between the fibers and the surrounding fluid the fiber concentration was increased in the near wall region. An increased concentration was found in a limited region close to half a fiber length from the wall. For the shorter fibers a large number of fibers was also detected in the very proximity of the wall.

1. Introduction

Suspensions of fibers are encountered in several engineering applications such as pharmaceutical applications, food processing, waste water treatment, composite processing and paper manufacturing. The final orientation distribution in the latter example is highly dependent on the suspension flow at an early stage of the process. As fibers travel with a suspension they will interact with the fluid, with each other and with the boundaries of the flow. This experimental study focuses on how fibers are oriented when they flow close to a solid wall.

A single fiber suspended in a linear shear flow will rotate due to the fluid motion. The flow situation is illustrated in figure 1. In this figure, the coordinates (x, y, z), the angles ϕ and θ defining the orientation of the fiber and the linear shear flow $\mathbf{u} = \dot{\gamma} y \mathbf{e}_x$ are defined. The angle β from the flow direction to the projection of the major axis of the fiber in the xz-plane is also shown.

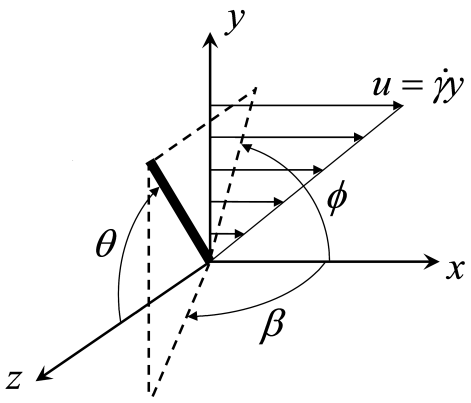

FIGURE 1. Coordinate system, velocity field and definitions of θ and ϕ used in Jeffery's analysis and β used for evaluation of the present data. The major axis of the fiber or spheroid is indicated with a thick line.

Jeffery (1922) derived the equations of motion for a spheroid suspended in a simple shear flow, assuming that inertia, both of the liquid and the spheroid, can be neglected. Under these assumptions, the rotation of the spheroid is described by

$$\dot{\phi} = -\frac{\dot{\gamma}}{r_e^2+1}\left(r_e^2\sin^2\phi + \cos^2\phi\right) \tag{1}$$

$$\dot{\theta} = \left(\frac{r_e^2-1}{r_e^2+1}\right)\frac{\dot{\gamma}}{4}\sin 2\phi \sin 2\theta, \tag{2}$$

where r_e is the spheroidal aspect ratio of the particle, *i.e.* the ratio between the major and minor axes. The period of the rotation is given by

$$T_J = \frac{2\pi}{\dot{\gamma}}\left(\frac{r_e^2+1}{r_e}\right). \tag{3}$$

Integration of equations (1) and (2) with respect to time t yields

$$\cot\phi = -r_e\cot\left(\frac{2\pi t}{T_J}+\phi_0\right) \tag{4}$$

$$\tan\theta = \frac{Cr_e}{(r_e^2\sin^2\phi+\cos^2\phi)^{1/2}}, \tag{5}$$

where the orbit constant C and the phase shift ϕ_0 are constants determined by the initial conditions. It has been shown experimentally that Jeffery's analysis form a good approximation for the motion of fibers suspended in viscous shear flows, *e.g.* Taylor (1923); Binder (1939); Trevelyan & Mason (1951); Anczurowski & Mason (1968). Thus, equations (1–5) are valid also for cylindrical

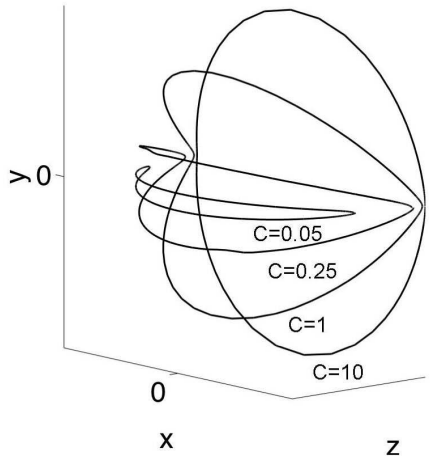

FIGURE 2. The path of a fiber end point for $r_e = 8$ and different C-values in Jeffery's equation.

fibers. This has also been shown analytically by Bretherton (1962). Furthermore, the equations are also valid in a paraboloidal flow if the shear rate is evaluated at the center of the particle, see Chwang (1975).

In order to use Jeffery's equations for cylindrical particles an equivalent spheroidal aspect ratio has to be used. The equivalent aspect ratio can be computed using the relation by Harris & Pittman (1975)

$$r_e = 1.14 r_p^{0.844}. \tag{6}$$

The geometrical aspect ratio is here denoted by $r_p = l/d$, where l and d are the full length and diameter of the fiber, respectively.

In figure 2 Jeffery orbits are shown for various values of C and $r_e = 8$. The curves show the orbit of a fiber end point for the indicated values of C. At the limit of zero inertia, a fiber will rotate in closed orbits around its center of mass and will stay in the same orbit for an indefinite time, *i.e.* $dC/dt = 0$. For $C = 0$ the major axis of the fiber is aligned with the vorticity axis, *i.e.* $\beta = 90$. The fiber spins around this axis, with the angular velocity $\dot{\gamma}/2$. For large values of C the fiber is oriented close to the flow direction most of the time, *i.e.* $\beta = 0$. Every half period there is a rapid increase in $\dot{\phi}$, which results in a quick 180 degrees flip around the vorticity axis.

Jeffery's orbits are often used as a starting point for phenomenological explanations of the motion of fibers in a suspension. However, fiber-fiber and fiber-wall interactions are not taken into account. The wall effect has been studied both experimentally by *e.g.* Stover & Cohen (1990); Moses, Advani &

Reinhardt (2001); Holm & Söderberg (2007); Carlsson, Lundell & Söderberg (2007) and numerically by *e.g.* Dabros (1985); Hsu & Ganatos (1989, 1994); Gavze & Shapiro (1997, 1998); Pozrikidis (2005). A general conclusion is that Jeffery's equations still form a good approximation, although with an increasing period of rotation closer to the wall.

Fibers with values of β close to 0, located closer to the wall than half a fiber length, have been observed by Stover & Cohen (1990) to interact with the wall in what is referred to as a pole vaulting motion. When performing this motion, a fiber end point hits the wall due to its rotation. This results in a movement away from the wall, to a point where the fiber center is located approximately half a fiber length from the wall. The orientation of the fiber is kept close to $\beta = 0$.

Holm & Söderberg (2007) and Carlsson *et al.* (2007) have studied the fiber orientation β close to a solid surface, where it has been observed that a considerable portion of the fibers tend to orient themselves perpendicular to the flow direction. For fibers rotating in Jeffery orbits the amplitude in the y-direction increases with increasing values of C, see figure 2. As a consequence the domain of possible Jeffery orbits, in the region $y < l/2$, is reduced. It was proposed by Carlsson *et al.* (2007) that the fibers move in Jeffery-like orbits also in the region near the wall and tend to adopt an orbit within the reduced domain. In the study it was also shown to be possible to influence the fiber motion near the wall by modifying the wall surface structure.

In the present study experimental measurements on flowing fiber suspensions with varying aspect ratios and concentrations will be presented. The fiber orientation β and concentration in planes parallel to a solid surface are analyzed. Compared to the earlier study by Holm & Söderberg the method for determining the wall normal position has been refined. Consequently, the orientation distribution near the wall is now better resolved. In addition, the concentration variation near the wall is now measured. The experimental apparatus and measurement techniques are described in section 2. This is followed by results and discussion in section 3. Finally the conclusions are given in section 4.

2. Experimental apparatus & technique

A CCD camera was used in order to visualize flowing fibers, in the proximity of a solid surface. Image analysis made it possible to find the velocity and orientation of the fibers in planes parallel to the solid surface. The velocity of the fibers and the wall normal velocity profile are used to determine their distance from the wall.

$r_p = l/d$	T [K]	ν [m^2/s]	ρ_f [kg/m^3]
7	295.5 ± 0.5	$(383 \pm 10) \cdot 10^{-6}$	1210 ± 15
30	295.5 ± 0.5	$(387 \pm 10) \cdot 10^{-6}$	1209 ± 15

TABLE 1. Temperature, kinematic viscosity and density of the liquid mixture in which the fibers were suspended.

2.1. *Fiber suspension*

The fiber suspension consisted of cellulose acetate fibers suspended in a viscous liquid. The density of the cellulose acetate fibers was $\rho_p \approx 1300$ kg/m^3. Experiments were conducted using two different aspect ratios, $r_p \approx 7$ and $r_p \approx 30$, where the diameter of the fibers was $d \approx 70$ μm and the length l of the fibers was cut to 0.5 and 2 mm, respectively. For each aspect ratio of the fibers two different concentrations were used. Expressed as the number of fibers to be found in a volume of l^3 these were $nl^3 \approx 0.01$ and 0.25 for $r_p \approx 7$ (cases A & B) and $nl^3 \approx 0.25$ and 2 for $r_p \approx 30$ (cases C & D).

The index of refraction of the fibers was approximately matched to that of the liquid. In order to visualize the fibers 100% of the fibers were dyed black for the low concentration cases (cases A & C). For the cases of higher concentration (cases B & D) only about 4% and 16% respectively of the fibers were dyed black.

The fibers do not deform in the present flow, but are to some extent permanently deformed. An analysis was made finding the tangents of the fiber end points on a set of fibers for both fiber lengths. From this analysis it is found that the curvature is smaller than 10 degrees for about 85% and 55% of the shorter and longer fibers, respectively.

The liquid phase was a mixture of polyethylene-glycol (PEG-400) and glycerine. The properties of the mixture for the two different aspect ratios are summarized in table 1. Note that the density of the liquid is lower than that of the fibers. The fibers will thus sediment slowly when suspended in the liquid.

2.2. *Flow apparatus*

In the experiments a film of the fiber suspension was flowing down an inclined glass plate. The thickness of the film was $h = 17.0 \pm 0.2$ mm for the cases when $r_p \approx 7$ and $h = 17.5 \pm 0.2$ mm when $r_p \approx 30$. A schematic figure of the test section is shown in figure 3. It is the same flow apparatus as the one used by Carlsson *et al.* (2007). The length of the channel was 1200 mm and the width was defined by an insert (the large gray area in figure 3), placed on the glass plate. From $x = 0$ mm to $x = 150$ mm there was a gradual change in the width, from 400 mm to 100 mm. For $x > 150$ mm the width was constant and equal to 100 mm. The coordinates are defined in figure 3.

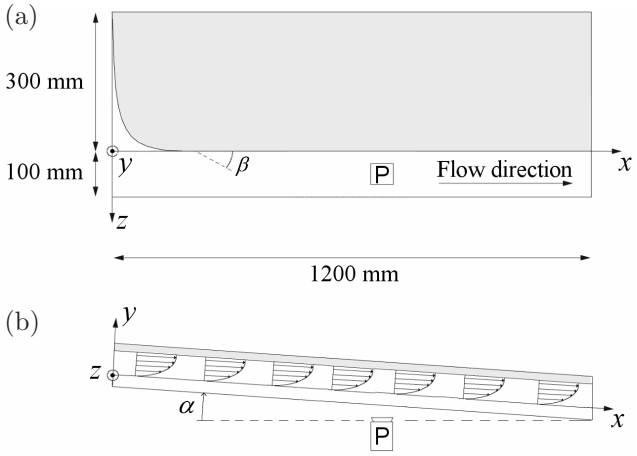

FIGURE 3. Schematic figure of the flow section, (a) Top view, (b) Side view. The camera position for orientation measurements is denoted by P.

The velocity in the x-direction of a Newtonian fluid film flowing down an inclined plane is given by

$$u = \frac{g}{2\nu} y(2h - y) \sin \alpha, \tag{7}$$

where g is the constant acceleration of gravity, ν is the kinematic viscosity of the fluid and y is the wall normal position, where $y = 0$ at the wall and $y = h$ at the free surface of the film. Furthermore α is the angle of inclination of the plane with respect to horizontal. In the present experiments $\alpha = 2.60 \pm 0.1$ degrees. Equation (7) can for instance be found in Acheson (1990).

It was shown previously by Carlsson *et al.* (2007) that the flow is fully developed and that there is no acceleration present in the flow. Typical velocity profiles are shown in figure 4. The velocity u and wall normal position y is normalized with the free surface velocity U_s and liquid sheet thickness h, respectively. The measurements were conducted on fibers with $r_p \approx 30$ at $nl^3 \approx 0.15$ and each dot represents the velocity and position of one fiber tracked through three consecutive images. The solid line is given by equation (7). The dashed lines denotes the minimum and maximum velocity based on the accuracies in measuring h, α and ν.

It is noted that there is some scatter in the data. A small fraction of the detected fibers have unphysical velocities which are due to mismatches in the particle tracking velocimetry algorithm, which will be explained briefly in the following section. For $x = 650$ mm in figure 4 (a) the fraction of erroneous velocities is as high as 14%, whereas for $x = 750$ and 850 mm in (b) and (c)

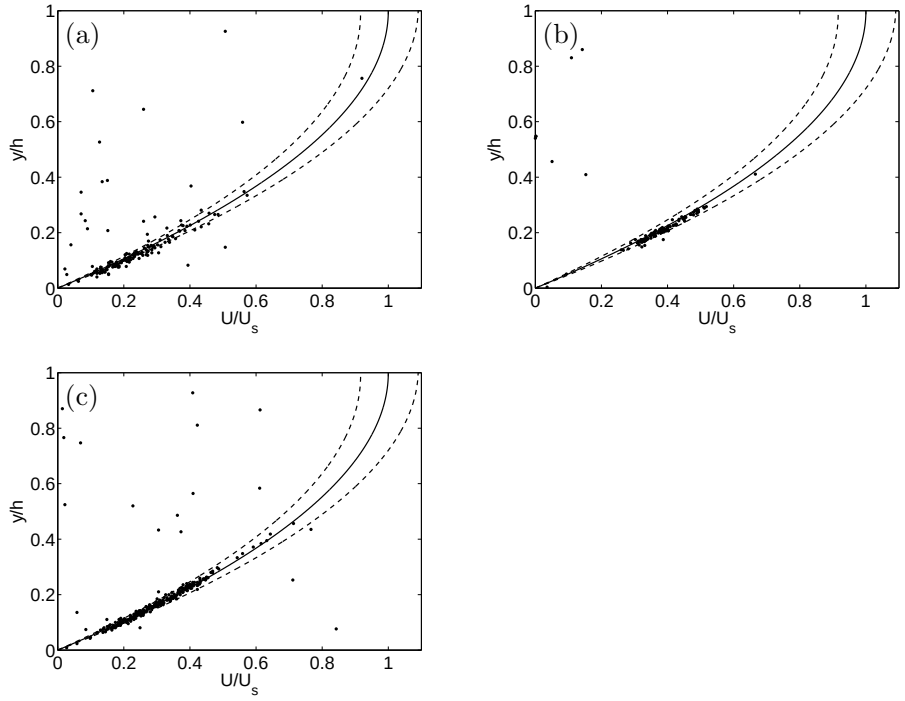

FIGURE 4. Velocity profile in the flow apparatus at $x = 650$, 750 and 850 mm in (a), (b) and (c), respectively.

the fraction is about 6%. Similar errors will be present also in the orientation measurements although less frequently. The reason for this is that the image quality is poorer in the velocity profile measurements, since the plane of focus of the camera is located about 5 cm into the suspension in comparison to only a couple of millimeters for the orientation measurements.

Disregarding the scattering, the measured velocities coincide well with the profile given by equation (7). This fact will be used to determine the distance to the wall of individual fibers in the orientation measurements.

2.3. *Measurement & analysis procedure*

2.3a. *Image capturing.* For the orientation studies the CCD camera was mounted underneath the glass plate at $x = 750$ mm (position P in figure 3). Images were captured, three at a time, with a frequency of $f = 5.13 \pm 0.05$ Hz when $r_p \approx 7$ and $f = 10.27 \pm 0.05$ Hz when $r_p \approx 30$. There was a delay of $T_s \approx 12$ s between every set of three images. The delay was implemented in order for the fibers to pass out of the field of view before the next set of three images was

captured. Therefore the exact length of T_s is not crucial. A total of 300 images per set of three images were captured for each fiber length and concentration. The field of view of the images was $X \times Z = 15 \times 20$ mm^2 for $r_p \approx 7$ and $X \times Z = 12 \times 17$ mm^2 for $r_p \approx 30$, where X and Z are the sizes of the image in the x- and z-directions, respectively.

2.3b. *Determination of fiber orientation.* The angle β is defined as the angle in the xz-plane taken clockwise from the flow direction (when viewed from above), figure 3. To determine the orientation β of the fibers a second order ridge detector within the class of steerable filters derived by Jacob & Unser (2004) was used. The filter has been evaluated for fiber detection in flowing suspensions by Carlsson, Lundell & Söderberg (2009).

2.3c. *Determination of fiber velocity.* In order to find the velocity of the fibers a particle tracking velocimetry (PTV) algorithm was used. The PTV-algorithm uses information concerning the location of individual fibers in three subsequent images. In order to indentify a particular fiber in the second image a rectangular area is generated with a chosen width and a length starting from the original fiber position to the end of the image in the streamwise direction. All fibers inside the rectangular area in the second image are considered as candidates of being the same as the original fiber. The distance from the original position to a candidate position is used to compute a position where the fiber should be in the third image if it is assumed to travel with the same velocity. If a fiber is detected sufficiently close to the computed position, for the candidate fiber, in the third and last image it is considered to be the same fiber as the original fiber.

Threshold values have to be set on the sizes of the areas in which fibers are searched for in the second and third image of the set. The width of the areas in the z-direction are $0.4l$ and $0.2l$ for the short and long fibers, respectively. The length in the streamwise direction x in the third image is of the same order of magnitude, but also varies with the velocity so that the length is increasing with the velocity. This is done in an attempt to reduce an under-representation of faster fibers.

Fibers found in a set of three images, with a velocity higher than X/T_s, will leave the field of view before the subsequent set of images are captured, independently on their location in the images. The velocity X/T_s corresponds to a distance from the wall of $y \approx d$. To ensure statistically independent data the x-position where the fibers has to be found in the images is set to be a function of the fiber velocity u_{fib}. If X_0 is the x-position farthest upstream in the images, the fiber has to be found in the region between X_0 and $X_0 + u_{fib}T_s$. In this manner the possibility of finding a fiber with a velocity lower than X/T_s, more than once, is eliminated. For further details, see Carlsson *et al.* (2007).

Case	$r_p = l/d$	nl^3	N
A	7	0.01	5933
B	7	0.25	5427
C	30	0.25	4825
D	30	2.0	6277

TABLE 2. Aspect ratio, concentration and number of detected fibers N for cases A-D.

2.3d. *Determination of fiber concentration.* The concentration of fibers at y is determined by the number of fibers N that is detected inside of the volume $V = \Delta X \Delta Y \Delta Z$. The concentration at $y = y_k$ can then be expressed as

$$c(y_k) = \frac{N\left(x \in [0, \Delta X], y \in [y_k - \Delta Y/2, y_k + \Delta Y/2], z \in [-\Delta Z/2, \Delta Z/2]\right)}{V}. \tag{8}$$

Here $\Delta Z = Z$ and ΔY can be chosen arbitrarily, with the help of equation (7), based on the desired resolution in the y-direction. The distance $\Delta X = X - 2u_{fib}/f$ is however a function of the fiber velocity, see Carlsson *et al.* (2007). This is due to the fact that the fibers have to be found in three subsequent images and that the fibers will travel a distance within the period it takes to capture these images. Hence, it is not possible to detect fibers of $u_{fib} > Xf/2$ since these fibers will have left the field of view, before the third of the three images is captured, independent on their location in the first image. In practise, this limits the maximum value of y where a fiber can be detected. It is also worth mentioning that the absolute value of the computed concentration is uncertain, mainly since it is strongly coupled to the threshold values set in the PTV.

3. Results & Discussion

Measurements from four cases (A, B, C & D) will be presented. The aspect ratios and concentrations of the cases are shown in table 2 together with the total number of fibers N for which the velocity and orientation have been determined in the region $0 < y/l < 1.5$. In the presented results the computed angular distribution at different distances from the wall is reported. The wall normal distribution of fibers is also shown.

3.1. *Period of rotation in near wall region*

The period of rotation close to the wall is measured manually for a small set of 23 individual fibers. This is done in order to validate that the fibers are rotating with a period in reasonable agreement with Jeffery's equations. A separate set of images were captured with the frequency $f = 5.13 \pm 0.05$ Hz for $r_p \approx 7$ and

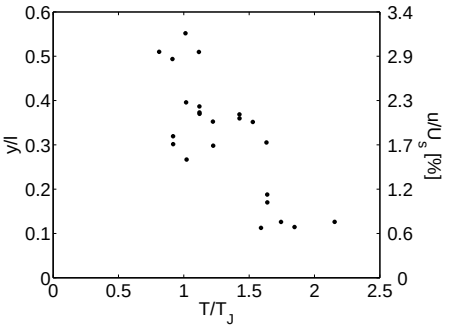

FIGURE 5. Period of rotation of individual fibers with $r_p \approx 7$ as a function of y.

$nl \approx 0.01$. The images are captured in the xz-plane. In order to measure the period of rotation it is necessary to detect a change in orientation of the fibers in the sequence of images. Therefore the period was only measured on fibers that have a minimum value of β between 30 and 60 degrees during its complete rotation. There are few longer fibers fulfilling this restriction why the period was only measured on short fibers. The velocity of the fibers was measured simultaneously in order to estimate the fiber's distance from the wall.

The results of the rotation period are shown in figure 5. Each dot in the figure denotes the measured period of rotation, normalized with the Jeffery period, of an individual fiber. The maximum error of T/T_J for a fiber is estimated to be about ± 0.4. The reason for the large error is partly due to the low frame rate of camera which can cause an error in the measured rotation. There is also a width distribution of the fibers that affects the Jeffery period used for normalization. Nevertheless, a trend can be seen. For distances from the wall about $y/l \approx 0.5$ the period is around the period given by Jeffery, which is reasonable. Closer to the wall the period increases to values large enough so that a fiber could not possibly rotate with the Jeffery period even with the relatively large error of T/T_J taken into account. An increased period of rotation near the wall is also consistent with earlier studies, *e.g.* Dabros (1985); Stover & Cohen (1990); Gavze & Shapiro (1997) and Pozrikidis (2005).

3.2. *Concentration variations in the wall-normal direction*

As mentioned previously the concentrations investigated were $nl^3 \approx 0.01$ and 0.25 for $r_p \approx 7$ (cases A & B) and $nl^3 \approx 0.25$ and 2 for $r_p \approx 30$ (cases C & D). These are the initial concentrations that one would expect to find if the fibers were homogenously distributed across the shear layer. In figure 6 the concentration $c(y)$, defined in equation (8), is shown. The concentrations

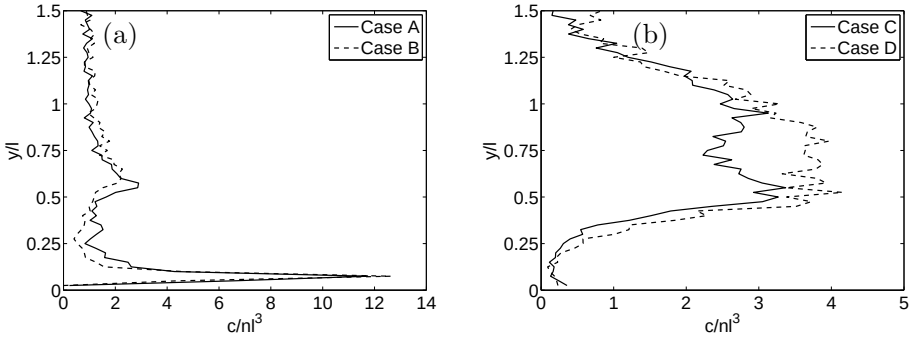

FIGURE 6. Variations in concentration as a function of the distance from the solid surface for fibers with $r_p \approx 7$ in (a) and $r_p \approx 30$ in (b).

have been normalized with their respective initial concentration, which is only approximative. Also, the obtained concentration level is partly coupled to threshold values set in the PTV-algorithm. Therefore the absolute values in figure 6 should be interpreted with some care. Nevertheless, the distribution of the fibers is similar for different threshold values. This is shown in figure 7 where the threshold values has been modified for cases B & C. The solid lines correspond to the original threshold values in the PTV-algorithm, upon which the results presented are based. The other two lines, the dot-dashed and the dashed, correspond to lower and higher threshold values, respectively. The new threshold values are set so that the areas, in which fibers are searched for in the PTV-algorithm, is roughly half or twice the areas of the original threshold values. The result is roughly 10-20% more or less detected fibers as compared to the original threshold values. The relative distribution of fibers is not highly dependent of the threshold values. Thus, conclusions can be drawn concerning the different characteristics of the concentration profiles seen for $r_p \approx 7$ and $r_p \approx 30$.

Returning to figure 6 it is seen that for all cases there is an increase in concentration near $y/l = 0.5$. It is likely that fibers sufficiently close to the wall will undergo a pole vaulting motion similar to the motion previously observed by Stover & Cohen. This should result in an increased concentration at about half a fiber length from the wall. From figure 6 it is clear that there is an increase in concentration for all cases near $y/l = 0.5$.

The accuracy of the velocity measurements is based on measurements of ν, α and h. Taking this into account there could be a small offset, constant for each respective case, in the determination of y. The distance from the peak of

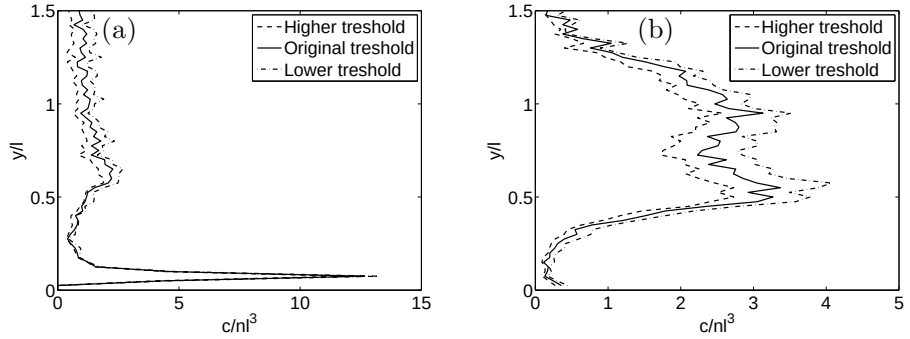

FIGURE 7. Variations in concentration as a function of y for different threshold values set in the PTV; (a) case B and (b) case C.

the increased concentration near half a fiber length from the wall to $y/l = 0.5$ is smaller than the estimated possible offset for all cases apart from case B.

For $r_p \approx 7$ in figure 6 (a) there are also a large number of fibers accumulated very close to the wall. The origin of this accumulation is clearly the density difference between the fibers and fluid. Still, the accumulation at the wall is only seen for the shorter fibers. There is a small trace of a local increase near the wall also for the longer fibers in (b) at the wall, but this increase is very small if compared with the peak for the shorter fibers.

3.3. *Angular distribution in near wall region*

The orientation distribution for all cases, at $x = 750$ mm, is shown in figure 8 for different distances from the wall, *i.e.* for different fiber velocities. The distance from the wall has been scaled with the fiber length l. In order to compensate for a varying wall normal concentration the orientation distribution is normalized at each distance from the wall. The darker regions in the graphs indicate where the fraction of fibers is large. Below the solid line it is not possible for a fiber to complete any undisturbed Jeffery orbit without hitting the wall.

Due to the positive streamwise rate-of-strain in the upstream contraction, between $x = 0$ and $x = 150$ mm, the fibers will initially tend to align with the flow direction ($\beta = 0$). It is clear for all cases that for distances farther away from the wall than half a fiber length most of the fibers have stayed close to the flow direction. As the distance is decreased below $y/l = 0.5$ the shorter fibers in (a) and (b) are detected above the solid line, where it is possible to rotate in Jeffery orbits. In the very proximity of the wall the fibers are oriented close to perpendicular to the flow direction. Also for the longer fibers a change in orientation is observed near the wall. When interpreting (c) and (d) near the

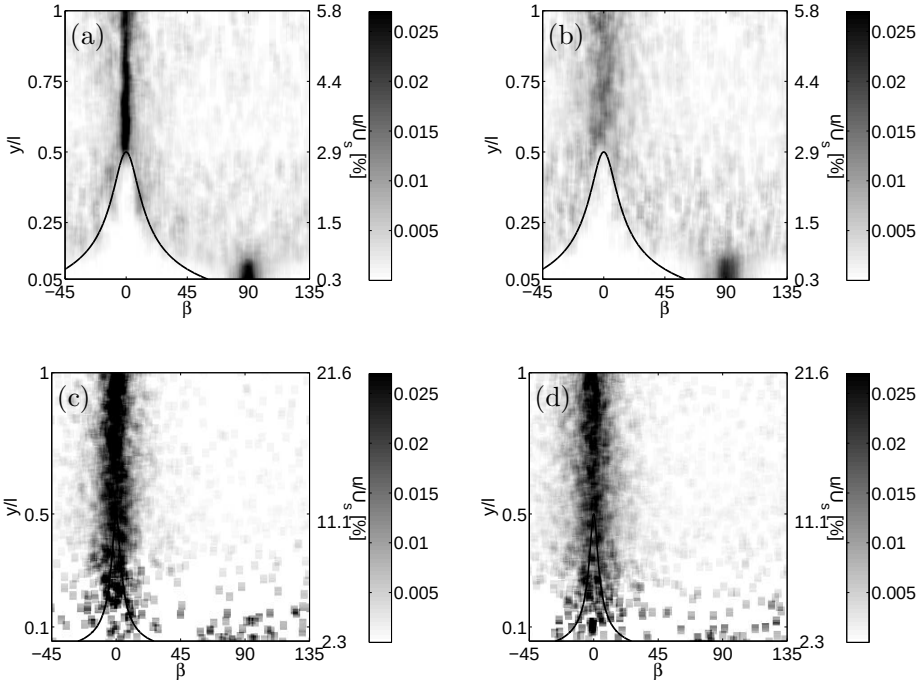

FIGURE 8. Fraction of fibers as a function of β for different distances from the wall; (a) $r_p \approx 7$, $nl^3 \approx 0.01$, (b) $r_p \approx 7$, $nl^3 \approx 0.25$, (c) $r_p \approx 30$, $nl^3 \approx 0.25$ and (d) $r_p \approx 30$, $nl^3 \approx 2.0$. The distribution of fibers is normalized at each y-position.

wall it should be kept in mind that the statistics is weak here due to the low concentration. Still, some of the longer fibers are detected in the region below the solid line.

In order to investigate the significance of the fibers detected below the line in figure 8 (c) and (d) a manual inspection was made of the images. Twenty of the fibers located below the line in 8 (c) were investigated. Fifteen of these fibers were found to have a curvature of the order 10 to 20 degrees. Two of the fibers were mismatches in the PTV where the velocity is based on different fibers in the set of three subsequent images. Two other fibers were located so close to the line so that they might as well be interpreted to be on the line or slightly above. The remaining fiber was a fiber with $r_p \approx 7$ which had remained in the system after the previous measurements. The curved fibers tended to be detected in the region above $y/l = 0.2$ where the angular spacing to the solid

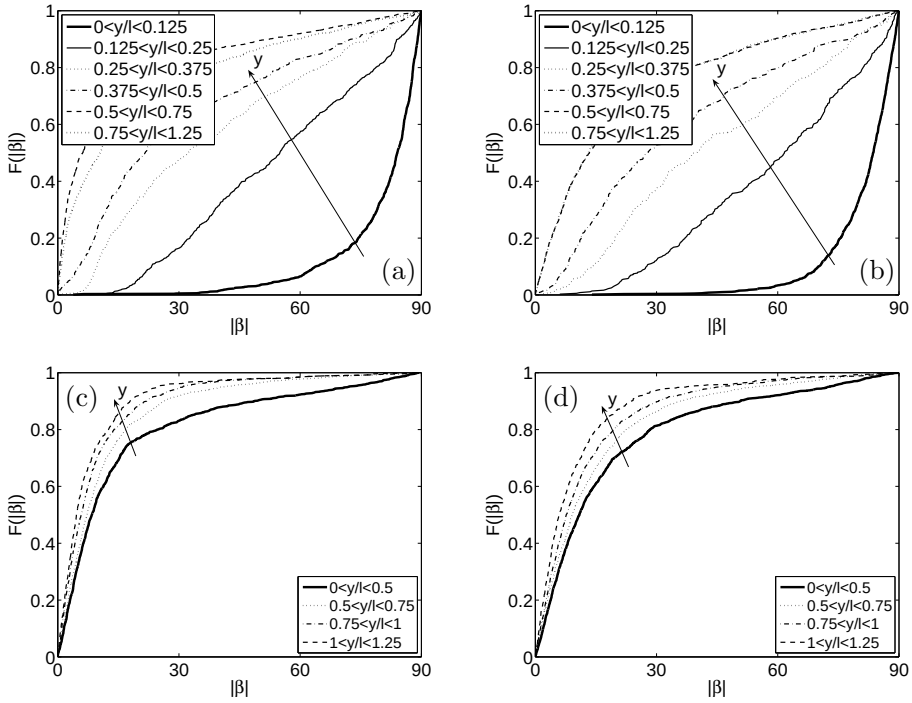

FIGURE 9. Distribution function $F(|\beta|)$ at different distances from the wall; (a) case A, (b) case B, (c) case C and (d) case D.

line is relatively small. Concluding, no straight fiber was detected in an area where it could not rotate in a Jeffery orbit without hitting the wall.

Detailed information on the orientation of the fibers is given by the distribution function $F(|\beta|) = P(B \leq |\beta|)$, defined as the probability that a fiber will be oriented between the flow direction and a given angle $|\beta|$. The distribution function is shown in figure 9 for all cases. The figures illustrate how $F(|\beta|)$ varies with the distance from the solid surface. In figure 9 (a) and (b), $r_p \approx 7$, it is seen that for distances farther away from the wall than half a fiber length the majority of the fibers are still oriented close to the flow direction, since F increases rapidly at $|\beta| = 0$. However, as soon as the fibers are located closer to the wall than half a fiber length $F(|\beta|)$ changes character. A gradual change towards a more isotropic distribution occurs as the distance from the wall is decreased to $y/l \approx 0.25$. When the distance is decreased even more the fibers tend to orient themselves close to perpendicular to the flow direction in the region $0 < y/l < 0.125$.

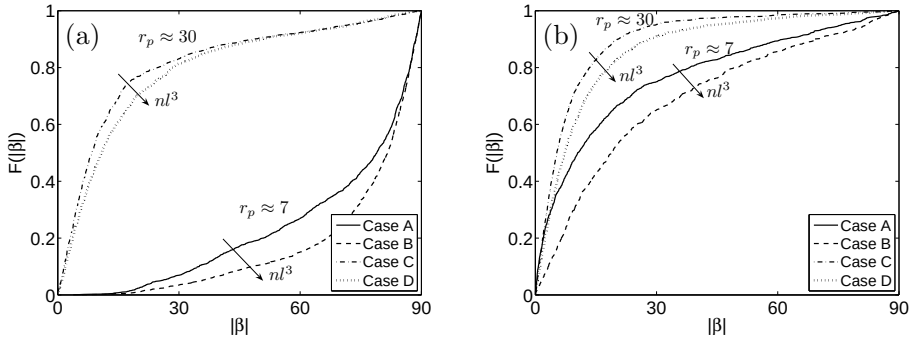

FIGURE 10. Distribution function $F(|\beta|)$ for all cases: (a) in the region $0 < y/l < 0.5$ and (b) in the region $0.75 < y/l < 1.25$.

The angular distribution at different y-positions, for fibers with aspect ratio $r_p \approx 30$, are presented in figure 9 (c) and (d). Due to the limited statistics near the wall the resolution is reduced as compared to the shorter fibers. The distributions show that the fibers are fairly aligned with the flow direction for all cases, although the fibers tend to be less aligned when the distance to the wall is decreased.

The differences and similarities between the cases are highlighted in figure 10. $F(|\beta|)$ is shown for all cases in two different regions; close to the wall, $0 < y/l < 0.5$, in (a) and about one fiber length from the wall, $0.75 < y/l < 1.25$, in (b). The longer fibers are clearly more aligned than the short fibers in both regions. A small effect is also noted for a change in concentration; for both aspect ratios the fibers tend to adopt slightly higher values of β for an increasing concentration. This could perhaps be attributed to fiber-fiber interactions.

3.4. *Physical mechanisms for drift in fiber orientation*

It is seen in figure 8 (a) and (b) that the shorter fibers tend to adopt an orientation that makes it possible to rotate in Jeffery orbits also near the wall. It is also clear from figure 6 that the shorter fibers tend to accumulate at the wall. In order for a fiber, initially at some distance from the wall, to end up at the wall there has to be a migration in orientation as the wall is approached. In other words, there has to be a physical mechanism that affects the fiber orientation so that a fiber, initially oriented close to the flow direction, can end up oriented close to perpendicular to the flow when it reaches the wall.

In this section the order of magnitude of inertial and sedimentation effects will be considered leading to the results in figure 12. The experimental results

indicate that the fibers are rotating in a manner close to the solution of Jeffery (1922). It is therefore assumed that this will be the base motion and that inertia and sedimentation will only cause a small deviation from the solution. The drift in orientation in the present experiments will be estimated based on theoretical predictions on inertial and sedimentation effects by Subramanian & Koch (2005) and Carlsson & Koch (2009).

3.4a. *Drift due to sedimentation towards the wall.* Due to the density difference between the fibers and the fluid, the fibers will sediment slowly. As a sedimenting fiber approaches a wall the velocity disturbance of the fluid, due to the presence of the fiber, will be reflected by the wall. This causes the fiber to rotate towards the xz-plane, *i.e.* towards an orientation parallel to the wall. Carlsson & Koch (2009) estimated this rotation for a large aspect ratio fiber in a wall-bounded shear flow. This was done by introducing a mirrored image fiber in order to ensure that the vertical velocity component at the wall is equal to zero. The rotation of a fiber nearly aligned with a wall as it sediments towards the wall in an otherwise quiescent fluid was found to be

$$\dot{\phi}_{wr} = \frac{3\phi\Delta\rho g V}{2\pi\mu l^2}\left[\frac{16y_*^2}{3} - \left(1+4y_*^2\right)^{1/2}\left(\frac{8y_*}{3}+\frac{1}{6y_*}\right) + y_* \ln\left[\frac{(1+4y_*^2)^{1/2}+1}{(1+4y_*^2)^{1/2}-1}\right]\right], \tag{9}$$

where y_* is the distance from the wall of the fiber center normalized with l. Furthermore, μ, V and $\Delta\rho$ is the dynamic viscosity of the fluid, the volume of the fiber and the density difference between the fiber and fluid, respectively. The angles ϕ and θ are defined in figure 1.

Due to the linearity of the problem the principle of superposition applies to the rotation of the fiber. Therefore, as long as there is no wall contact, equation (9) estimates the additional rotation rate of a fiber in a shear flow, when it is oriented close to the xz-plane. A fiber rotating in a Jeffery orbit spends most of its time nearly aligned with the xz-plane. Therefore it is reasonable to expect that most of the orbit drift takes place when the fiber is oriented close to this plane. A more detailed justification of this assumption is given by Carlsson & Koch. A consequence of the fiber being nearly parallel to the wall is also that the rate of change of θ due to the wall reflection $\dot{\theta}_{wr} << \dot{\phi}_{wr}$ and it is therefore not considered.

Carlsson & Koch also introduced a local contact force at one of the fiber end points to model the situation when contact occurs between the wall and the fiber. Both a no slip and a free slip condition for the wall contact were considered. The additional rotation rate from the model was found to be

$$\dot{\phi}_c^{ns} = K^{ns}\left[\frac{3\ln(2r_p)\cos\phi}{8\pi\mu l^2\sin\theta}\Delta\rho g V\right] \tag{10}$$

$$\dot{\theta}_c^{ns} = K^{ns}\left[\frac{3\ln(2r_p)\cos\theta\sin\phi}{8\pi\mu l^2}\Delta\rho g V\right], \tag{11}$$

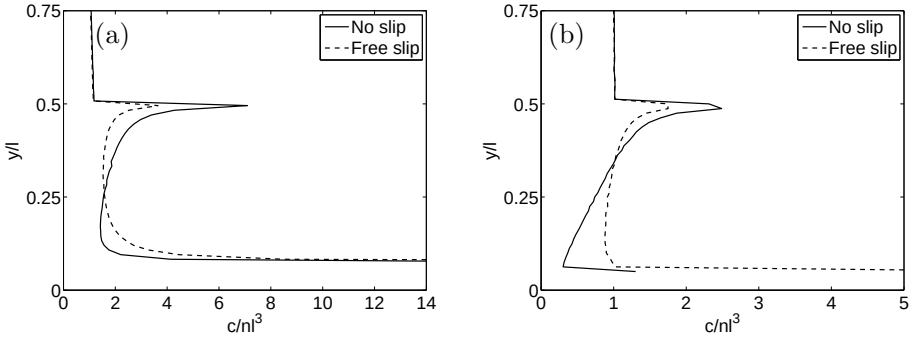

FIGURE 11. Computational concentration profiles with no slip and free slip wall contact condition for (a) $r_p \approx 7$ and (b) $r_p \approx 30$.

for a no slip condition applied for the fiber end point in contact with the wall and

$$\dot{\phi}_c^{fs} = K^{fs}\left[\frac{3\dot{\gamma}\sin^2\theta\sin^2\phi(\sin^2\phi-1)}{2(\sin^2\theta\sin^2\phi-2)} + \frac{3\ln(2r_p)}{4\pi\mu l^2}\Delta\rho g V\frac{(1+\sin^2\theta\sin^2\phi)(1-\sin^2\phi)}{\sin\theta\cos\phi(2-\sin^2\theta\sin^2\phi)}\right] \tag{12}$$

$$\dot{\theta}_c^{fs} = K^{ns}\left[\frac{3\dot{\gamma}\sin^3\theta\cos\theta\sin^3\phi\cos\phi}{2(2-\sin^2\theta\sin^2\phi)} + \frac{3\ln(2r_p)}{4\pi\mu l^2}\Delta\rho g V\frac{\cos\theta\sin\phi(1+\sin^2\theta\sin^2\phi)}{(2-\sin^2\theta\sin^2\phi)}\right] \tag{13}$$

for a free slip condition. The parameters K^{ns} and K^{fs} are non-zero and equal to one only when the fiber end point is in contact to the wall.

It was shown that both the rotation due to the wall reflection and due to the wall contact causes a migration towards lower values of the Jeffery orbit constant C, *i.e.* towards higher values of β. In a comparison of the model with the present experimental data, for fibers with $r_p \approx 7$, a qualitative agreement was found in that there was an accumulation of fibers oriented perpendicular to the flow direction at the wall.

In order to estimate the concentration profile a large number of fibers is chosen at the inlet of the channel. The concentration is initially assumed to be $c/nl^3 = 1$ for all y-positions. The initial orientation distribution is found by

using the relation

$$f(C) = \frac{RC}{\pi \left(4RC^2 + 1\right)^{3/2}}, \tag{14}$$

derived by Rahnama, Koch & Shaqfeh (1995) to be a steady state orientation distribution for dilute and semi-dilute aspect ratios in the limit of large aspect ratio. In equation (14) R is a fitting parameter. Here R is chosen so that the single moment $\langle \cos^2 \beta \rangle$ of the β-distribution is the same as for the experiments. Only fibers detected at $y/l > 1$ and $y/l > 0.5$ for $r_p \approx 7$ and 30, respectively, is used to find R. This results in $R \approx 0.57$ and 0.97 for the fibers with $r_p \approx 7$ and 30, respectively.

In figure 11 the computational concentration profiles are shown. For the shorter fibers in (a) the profiles for the no slip and free slip condition are qualitatively similar to the experimental profiles for cases A and B shown in figure 6 (a). There is an increased concentration at the wall and also at $y/l \approx 0.5$ due to a pole-vaulting-like motion occurring as a result of the wall contact conditions. For the longer fibers in 11 (b) there is a peak at $y/l \approx 0.5$ and there is also an increase in concentration near the wall. The local increase in concentration near the wall for case C and D in figure 6 (b) seems a bit small to be explained when only taking into account the sedimentation according to Carlsson & Koch.

3.4b. *Drift due to fluid inertia.* Since fewer fibers are detected at the wall than expected for fibers with $r_p \approx 30$, when taking sediment effects into account, this suggests that there may be at least one additional physical mechanism acting in the experiments. It has been shown in earlier studies (Qi & Luo 2003; Subramanian & Koch 2005, 2006; Altenbach *et al.* 2007) that both fluid and particle inertia are expected to drift a fiber, suspended in a simple shear flow, towards a final orientation in the xy-plane, *i.e.* towards $\beta = 0$. In this plane the fiber will spend most of its time close to the flow direction. Since inertia will tend to rotate the fibers towards the xy-plane this could potentially prevent the drift in orientation towards the vorticity axis, due to sedimentation towards the wall. Near the wall in the experiments, a particle Reynolds number $Re_d = \dot{\gamma} l^2/\nu$ based on the full length l of the fiber, is about 0.01 and 0.2 for fibers with $r_p \approx 7$ and 30, respectively. Although Re_l appear small also for $r_p \approx 30$ it could be large enough to slow down or possibly even prevent a weak drift towards the vorticity axis.

The magnitude of inertial effects can be estimated based on the work of Subramanian & Koch (2005). They examined the motion of a fiber suspended in a simple shear flow, for a small but finite Re_l. The fiber is assumed to be slender and the particle Reynolds number based on the diameter of the fiber $Re_d = \dot{\gamma} l d/\nu$ is considered negligible. As mentioned one result of their study is that a small Re_l will tend to drift the rotating fiber towards the xy-plane and

$\beta = 0$. From Subramanian & Koch the additional rotation rate of a fiber due to fluid inertia in a simple shear flow is given by

$$\dot{\phi}_{in} = -\frac{\dot{\gamma} Re_l}{16 \ln(r_p)} \sin^2\theta \sin 2\phi \left(\frac{1}{3} - \frac{7}{15} \cos^2\phi \right) \tag{15}$$

$$\dot{\theta}_{in} = \frac{7\dot{\gamma} Re_l}{120 \ln(r_p)} \sin^3\theta \cos\theta \sin^2\phi \cos^2\phi. \tag{16}$$

3.4c. *Estimation of drift in orientation.* Equations (9–15) estimates the drift in orientation due to sedimentation towards the wall and fluid inertia. An approximation of the total rate of rotation is now:

$$\dot{\phi} = \dot{\phi}_{jef} + \dot{\phi}_{wr} + \dot{\phi}_c + \dot{\phi}_{in} \tag{17}$$

$$\dot{\theta} = \dot{\theta}_{jef} + \dot{\theta}_c + \dot{\theta}_{in}, \tag{18}$$

where $\dot{\phi}_{jef}$ and $\dot{\theta}_{jef}$ is Jeffery's equations defined in equations (1) and (2). Since the terms from sedimentation and inertia are small, a fiber is not expected to deviate far from a Jeffery orbit in one period. Therefore it is convenient to study how the orbit constant C, introduced in equation (5), changes with time. This is shown in figure 12 for different initial orbit constants C_0 and initial distances y_0 from the wall. The results for fibers with $r_p \approx 7$ is shown in (a) and (b) for the no slip and free slip wall contact condition, respectively. In (c) and (d) the results for $r_p \approx 30$ is shown for both wall contact conditions. On the horizontal axis β_{0min} is the minimum absolute value of β over a complete period that a fiber with the initial orbit constant C_0 obtains.

The solid lines in the figure show where $dC/dt = 0$, or more accurately where the change of C over half a period of rotation is zero. Below the solid line $dC/dt < 0$, since the estimated effect due to wall reflection and wall contact is larger than the effect of fluid inertia, resulting in a total drift towards larger values of β. Above the solid line $dC/dt > 0$ resulting in gradually smaller values of β. The dashed lines shows the minimum value of β for a fiber rotating in Jeffery orbits without hitting the wall. If a fiber is located below the dashed line the fiber will make contact with the wall during the flip and the wall contact is included in the computations. It is emphasized that the figure indicates the sign of dC/dt over half a period of rotation at various initial conditions. As time evolves a fiber will change both its orientation and wall normal position. Above the dashed line a fiber will always sediment towards lower values of y. However, it will never be allowed to sediment far below the dashed line since it will continuously be pushed up to the dashed line in each flip around the vorticity axis due to the wall contact.

It is seen in figure 12 (a) and (b) that the results with no slip and free slip are identical for the short fibers. Recall that only the sign of dC/dt is shown in the figure. The values of dC/dt will differ in the region on and below the dashed line where the wall contact is included in the computations. The fact

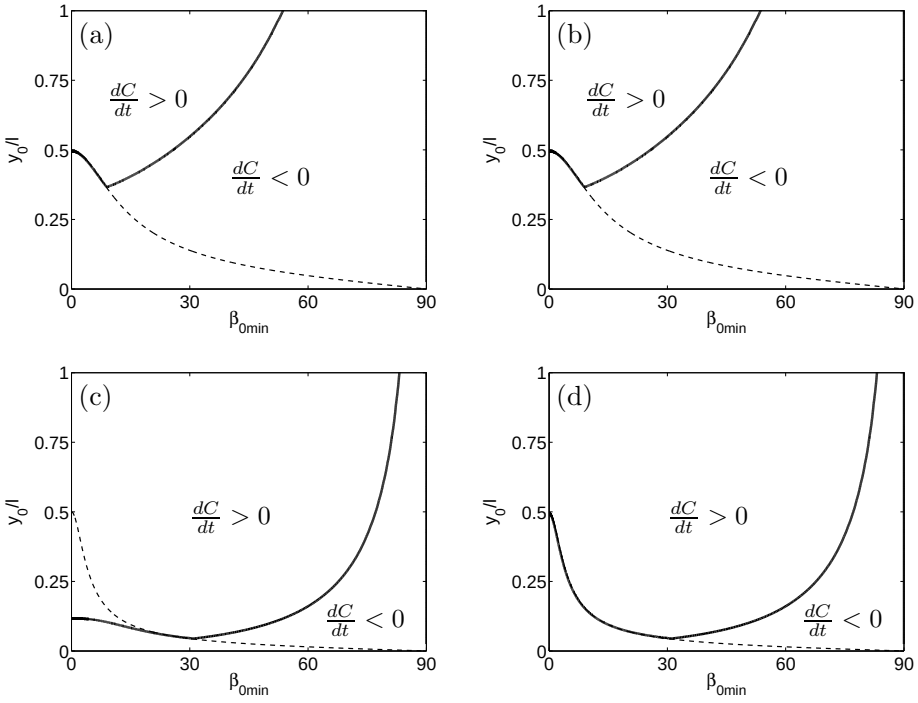

FIGURE 12. The sign of the orbit drift for different inital orientations and distances from the wall. The solid line indicates where $dC/dt = 0$ and below the dashed line a fiber will make wall contact during its flip around the vorticity axis. Fibers with $r_p \approx 7$ with (a) no slip condition and (b) free slip condition during wall contact. Fibers with $r_p \approx 30$ with (c) no slip condition and (d) free slip condition.

that (a) and (b) are the same just shows that the wall contact, for both the no slip and free slip condition, causes an orbit drift strong enough to make the total change of C over half a period of rotation to be negative. This is the case for all orientations of a fiber, *i.e.* as soon as a fiber has sedimented down to a distance from the wall where wall contact occurs the fiber will take on lower values of C. After a sufficient amount of time the fiber will be located at the wall oriented along the direction of vorticity. This could explain the increased number of fibers at the wall oriented close to perpendicular to the flow direction for case A and B in the experiments.

Looking at figure 12 (c) for $r_p \approx 30$, with the no slip condition implemented in the contact, the results are quite different as compared to (a) and (b). For

a longer fiber Re_l is larger and the inertial term is larger in the computations. Therefore dC/dt is positive in a larger fraction of the space shown in the figure. A feature worth noticing is that the thick line crosses the dashed line in 12 (c). This indicates that even after a fiber with small values of β_{min} has sedimented down to a y-position where wall contact occurs it will not tend to adopt lower values of C. Consequently, the fiber would not be expected to settle all the way down to the wall since it will stay close to the dashed line and β will not tend to increase but rather decrease.

Possibly this could explain the absence of fibers with $r_p \approx 30$ near the wall in figure 6. However, when implementing the free slip condition, which causes a stronger drift towards lower C than the no slip condition, the situation is changed. This is shown in figure 12 (d) where it is seen that for this case a fiber takes on lower values of C as soon as the wall contact is included in the computations, similar to the situation in (a) and (b).

The nature of the fiber-wall contact and how well the two implemented models capture the fiber dynamics is presently not clear. A slender body approach was used by Carlsson & Koch to estimate the rotation and translation of the fiber near the wall. In order to obtain a more accurate description, it may be necessary to take into consideration that the fiber has a finite thickness when one of the fiber end points is positioned very close to the wall.

4. Conclusions

In a slowly sedimenting fiber suspension flowing down an inclined wall, the fiber orientation has been analyzed in planes parallel to the wall. Due to an upstream contraction of the flow the fibers were initially oriented close to the flow direction. Farther downstream this orientation was still found to be the most probable for distances larger than half a fiber length from the wall. For fibers with $r_p \approx 7$ a clear change in the orientation distribution is found closer to the wall. At distances farther from the wall than $y/l \approx 0.5$ most of the fibers are close to aligned with the flow and at distances closer to the wall than about an eighth of a fiber length most of the fibers are oriented perpendicular to the flow direction.

An increased concentration of fibers was also found near the wall due to the sedimentation. A large fraction of the shorter fibers with $r_p \approx 7$ were found at the wall. This was not the case for fibers with $r_p \approx 30$ where most of the fibers were detected at distances farther from the wall than about half a fiber length. The fiber orientation results are in qualitative agreement with the studies by Holm & Söderberg (2007) and Carlsson *et al.* (2007). Also in these studies fibers were detected at orientations close to perpendicular to the flow direction in the near wall region. Carlsson *et al.* only performed measurements on one fiber suspension with $r_p \approx 7$ and $nl^3 \approx 0.25$ and in comparison to Holm & Söderberg more statistics have been added and a more accurate method to determine the fiber distance from the wall has been used.

Sedimentation towards the wall and fluid inertia have been presented as two physical mechanisms that could influence the orientation of fibers in the presence of a wall. An estimation of the drift in orientation of a fiber was performed based on theoretical predictions by Subramanian & Koch (2005) and Carlsson & Koch (2009). A likely reason for the accumulation of fibers oriented perpendicular to the flow direction for $r_p \approx 7$ is the density difference between the fibers and the fluid. When a fiber sediments towards the wall the reflection of the fluid velocity disturbance and the wall contact during the flip causes the fiber to migrate towards lower values of C (larger values of β). On the other hand fluid inertia will tend to drift the orientation so that C increases with time. This is presented as a possible reason to why few fibers in the experiments with $r_p \approx 30$ are found at the wall.

It should also be recalled that the wall normal distance of the fibers have been normalized with the fiber length. Therefore, the residence time of a fiber at y/l, will be about four times longer for fibers with $r_p \approx 7$ as compared to fibers with $r_p \approx 30$. Another difference is that the number of completed periods of rotation will be about 16 times as many for a fiber with $r_p \approx 7$ at y/l than for a fiber with $r_p \approx 30$, since T_J is almost linearly proportional to r_p from equation (3). Since the residence time is shorter and the number of rotation periods is less, for fibers with $r_p \approx 30$, it is also reasonable to expect that less fibers have time to settle to the wall.

Still, the difference in the amount of detected fibers at the wall appears surprisingly large. An experiment where the longer fibers have time to complete more periods of rotation is needed in order to verify the presented hypothesis of competition between (*i*) sedimentation towards the wall, wall contact and (*ii*) fluid inertia. The results suggest that the combined effect of sedimentation towards the wall and fluid inertia could be a focus area of future studies.

Acknowledgments

The authors acknowledge helpful discussions with Professor Donald L. Koch and Dr. Richard Holm. This work has been supported by the European Union FP6 project EcoTarget, contract number 500345 (NMP2-CT-2004-500345) (AC and FL) and by the Swedish Research Council, contract number VR-2005-5816 (FL).

References

Acheson, D. J. 1990 *Elementary Fluid Dynamics*, 38–40. Oxford University Press.

Altenbach, H., Naumenko, K., Pylypenko, S. & Renner, B. 2007 Influence of rotary inertia on the fiber dynamics in homogenous creeping flows. *Z. Angew. Math. Mech* **87** (2), 81–93.

Anczurowski, E. & Mason, S. G. 1968 Particle motions in sheared suspensions. XXIV. Rotation of rigid spheroids and cylinders. *Trans. Soc. Rheology* **12** (2), 209–215.

Binder, R. C. 1939 The motion of cylindrical particles in viscous flow. *J. Appl. Phys.* **10**, 711–713.

Bretherton, F. P. 1962 The motion of rigid particles in a shear flow at low Reynolds number. *J. Fluid Mech.* **14**, 284–304.

Carlsson, A. & Koch, D. L. 2009 Orbit drift of a slowly settling fiber in a wall-bounded shear flow. Manuscript in preparation.

Carlsson, A., Lundell, F. & Söderberg, L. D. 2007 Fiber orientation control related to papermaking. *J. Fluids Eng.* **129** (4), 457–465.

Carlsson, A., Lundell, F. & Söderberg, L. D. 2009 Evaluation of steerable filter for detection of fibres in flowing suspensions. Manuscript in preparation.

Chwang, A. T. 1975 Hydrodynamics of low-Reynolds-number flow. Part 3. Motion of a spheroidal particle in quadratic flows. *J. Fluid Mech.* **72**, 17–34.

Dabros, T. 1985 A singularity method for calculating hydrodynamic forces and particle velocities in low-Reynolds-number flows. *J. Fluid Mech.* **156**, 1–21.

Gavze, E. & Shapiro, M. 1997 Particles in a shear flow near a solid wall: Effect of nonspherity on forces and velocities. *Int. J. Multiphase Flow* **23** (1), 155–182.

Gavze, E. & Shapiro, M. 1998 Motion of inertial spheroidal particles in a shear flow near a solid wall with special application to aerosol transport in microgravity. *J. Fluid Mech.* **371**, 59–79.

Harris, J. B. & Pittman, J. F. T. 1975 Equivalent ellipsoidal axis ratios of slender rod-like particles. *J. Coll. Interf. Sci.* **50** (2), 280–282.

Holm, R. & Söderberg, D. 2007 Shear influence on fibre orientation. *Rheol. Acta* **46**, 721–729.

Hsu, R. & Ganatos, P. 1989 The motion of a rigid body in viscous fluid bounded by a plane wall. *J. Fluid Mech.* **207**, 29–72.

Hsu, R. & Ganatos, P. 1994 Gravitational and zero-drag motion of a spheroid adjacent to an inclined plane at low Reynolds number. *J. Fluid Mech.* **268**, 267–292.

Jacob, M. & Unser, M. 2004 Design of steerable filters for feature detection using Canny-like criteria. *IEEE T. Pattern Anal.* **26** (8), 1007–1019.

Jeffery, G. B. 1922 The motion of ellipsoidal particles immersed in a viscous fluid. *Proc. Roy. Soc. London A* **102** (715), 161–179.

Moses, K. B., Advani, S. G. & Reinhardt, A. 2001 Investigation of fiber motion near solid boundaries in simple shear flow. *Rheol. Acta* **40**, 296–306.

Pozrikidis, C. 2005 Orbiting motion of a freely suspended spheroid near a plane wall. *J. Fluid Mech.* **541**, 105–114.

Qi, D. & Luo, L. S. 2003 Rotational and orientational behaviour of three-dimensional spheroidal particles in Couette flows. *J. Fluid Mech.* **477**, 201–213.

Rahnama, M., Koch, D. L. & Shaqfeh, E. S. G. 1995 The effect of hydrodynamic interaction on the orientation distribution in a fiber suspension subject to simple shear flow. *Phys. Fluids* **7**, 487–506.

Stover, C. A. & Cohen, C. 1990 The motion of rodlike particles in the pressure-driven flow between flat plates. *Rheol. Acta* **29**, 192–203.

Subramanian, G. & Koch, D. L. 2005 Inertial effects on fibre motion in simple shear flow. *J. Fluid Mech.* **535**, 383–414.

Subramanian, G. & Koch, D. L. 2006 Inertial effects on the orientation of nearly spherical particles in simple shear flow. *J. Fluid Mech.* **557**, 257–296.

Taylor, G. I. 1923 The motion of ellipsoidal particles in a viscous fluid. *Proc. Roy. Soc. London A* **103**, 58–61.

Trevelyan, J. & Mason, S. G. 1951 Particle motions in sheared suspensions I. Rotations. *J. Colloid Sci.* **6**, 354–367.